ISSN 0005-1144
ATKAFF 51(3), 221–232(2010)

Božo Terzić, Goran Majić, Alojz Slutej

Stability Analysis of Three-Phase PWM Converter with LCL Filter by Means of Nonlinear Model

UDK 621.314.5:621.376.6
IFAC 5.5.4; 3.1.1

Original scientific paper

In this paper the stability problem of the three phase PWM converters with LCL filter without additional passive or active damping is analyzed. The system with the converter current feedback is considered where the stability problem is more acute. The analysis is performed using two theoretical methods, the discrete z-domain root locus technique and the nonlinear model simulation. The system with two different LCL filters is considered, one with the iron core inductors and the other with the air core inductors. In that way the influence of the iron losses on the system stability is investigated. It is shown that the stability margins obtained by means of the nonlinear model simulation are somewhat wider than the ones obtained by the root locus technique. The theoretical results are validated by the measurements performed on a 40 kW laboratory setup.

Key words: PWM converter, LCL filter, Stability, Root locus, Nonlinear model, Iron losses

Analiza stabilnosti trofaznog PWM energetskog pretvarača s LCL filtrom pomoću nelinearnog modela. U radu se analizira problem stabilnosti trofaznog PWM energetskog pretvarača s LCL filtrom bez dodatnog pasivnog ili aktivnog prigušenja. Razmatra se sustav s povratnom vezom po struji pretvarača gdje je problem stabilnosti izraženiji. Analiza je provedena koristeći dvije teorijske metode, geometrijsko mjesto korijena u diskretnom z-području i simulacija pomoću nelinearnog modela. Razmatran je sustav s dva različita LCL filtra, jedan koji koristi prigušnice sa željeznom jezgrom i drugi sa zračnim prigušnicama. Na taj je način istražen utjecaj gubitaka u željezu na stabilnost sustava. Pokazano je da su granice stabilnosti nešto šire kada se analizira stabilnost pomoću simulacijskog nelinearnog modela u odnosu na granice dobivene metodom geometrijskog mjesta korijena. Teorijski rezultati potvrđeni su mjerenjima koja su provedena na laboratorijskoj maketi nazivne snage 40 kW.

Ključne riječi: pretvarač s pulsno-širinskom modulacijom, LCL filter, stabilnost, geometrijsko mjesto korijena, nelinearni model, gubici u željezu

1 INTRODUCTION

In recent years, the three-phase grid-connected PWM converters with LCL-filters have gained much attention in the renewable energy sources and in adjustable-speed drives when the regenerative braking is required. Power regeneration, adjustable power factor and significantly less line current harmonic distortion are the most important advantages of this converter with respect to other types of converters. The LCL-filters are used for grid connections as they are more cost-effective compared to simple L-filters because smaller inductors can be used to achieve the same damping of the switching harmonics [1–4].

The main drawback of the LCL filter is a stability problem which appears because of the filter resonance effect. To overcome this problem it is possible to use damping resistors in series with the filter capacitors but this creates additional power losses [4]. An another solution is the active damping which is realized by modifying the control algorithm. Methods proposed in the literature differ in number of additional sensors and complexity of control algorithms [5–8]. Although the results presented in the papers show that the stability margins can be enlarged by the active damping, most of these methods have some restrictions and drawbacks such as a very complicated and unreliable parameter tuning and poor robustness against parameters variations.

It is clear that the precise determination of the stability margins of the PWM converter with LCL filters is very important. Experimentally determined stability margins can differ significantly in relation to the ones obtained by the theoretical analysis which is usually carried out in the discrete z-domain using root locus technique. Reasons for this are various such as the LCL filter model uncertainties, erroneous equivalent delays caused by the PWM and computation time, supply voltage distortion and line impedance variations [9–11].

From an industrial point of view it is desired to have a minimum number of sensors and therefore the control structure with only one set of the current sensors is preferred. Thereby either the line currents or the converter currents can be used as the current feedback signal [9, 11]. On the one hand, the use of the line current feedback is intelligible since the line power factor can be directly controlled. On the other hand, the converter current feedback is reasonable if the current sensors have to be built into the converter to protect it.

This paper focuses on the stability margins determination of the LCL-filter-based PWM converter with the converter currents feedback. The main scope is to investigate the system stability without any additional passive or active damping, i.e. if the only LCL filter inductors iron losses are sufficient to damp filter resonance oscillations. In addition, influence of the PWM pattern on the system stability is considered. The stability margins are investigated using theoretical and experimental procedures. Two theoretical approaches are used, z-domain root locus and nonlinear model simulation. Two different LCL filters are used to investigate the influence of the inductors iron losses on stability margins, the iron-core and air-core LCL filter.

System description and modeling are shown in Section 2 and a control overview is given in Section 3. The theoretical stability analyses using the discrete z-domain and nonlinear model respectively are shown in Section 4. The experimental results are presented and compared to the theoretical ones in Section 5.

2 SYSTEM DESCRIPTION AND MODELING

The analyzed system is shown in Fig. 1 and its parameters are listed in Table 1. A three-phase IGBT voltage source PWM converter is connected to the grid through the LCL filter. The PWM converter is loaded by a resistor or the inverter-fed induction machine. The supply voltages are measured for the purpose of synchronizing the control with the grid voltage. The control system requires both the dc link voltage and filter currents measurements.

Depending on the control structure, either the grid currents or the converter currents can be measured. In this paper, the control structure with the converter currents feedback is considered. The control algorithm is implemented in the digital signal controller.

2.1 Mathematical Model of LCL Filter with Iron Losses

For the stability analysis it is common to use the simplified LCL filter model neglecting the inductors iron losses [4, 5]. However, these losses make the system with converter current feedback to be more stable. As it is common, the iron losses are modeled with resistances connected in

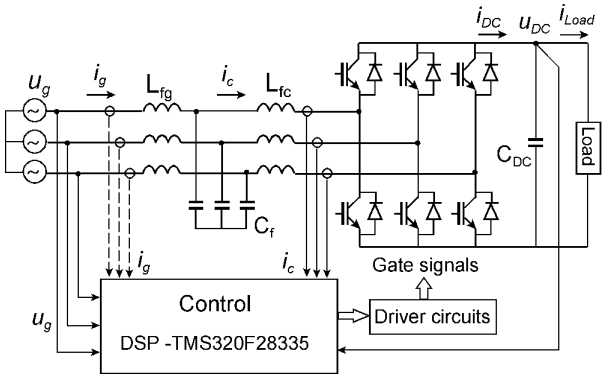

Fig. 1. PWM converter with LCL filter

Table 1. System parameters

Symbol	Quantity	Value
U_g	Nominal grid voltage (line-line, rms)	400 V
ω	Angular grid frequency	2π 50 Hz
I_g	Nominal filter current (rms)	60 A
L_{fg}	Inductance of grid-side filter inductors	0.6 mH
R_{fg}	Resistance of grid-side filter inductors	8 mΩ
L_{fc}	Inductance of converter-side inductors	1.8 mH
R_{fc}	Resistance of converter-side inductors	16 mΩ
C_f	Filter capacitance	60 μF
C_{DC}	DC link capacitance	2200 μF
f_s	Sampling and switching frequency	3 kHz
U_{DC}	DC link voltage	670 V

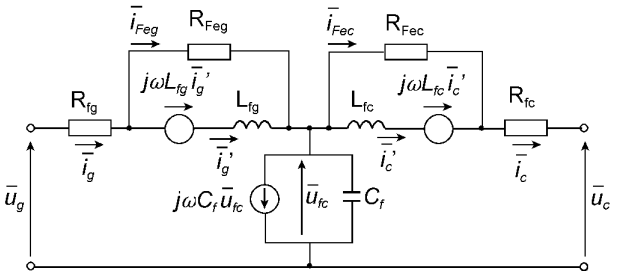

Fig. 2. Equivalent circuit of LCL filter

parallel to inductance. In that way, using the synchronous rotating reference frame, the LCL filter equivalent circuit shown in Fig. 2. is obtained. The LCL filter model is given in the synchronous rotating frame since the current control is done in the same reference frame with the d-axis aligned to the grid voltage space vector.

Based on the equivalent circuit shown in Fig. 2, the following LCL filter equations may be derived:

$$L_{fg}\frac{d\bar{i}_g'}{dt} = \bar{u}_g - \bar{i}_g R_{fg} - j\omega L_{fg}\bar{i}_g' - \bar{u}_{fc}$$

$$C_f\frac{d\bar{u}_{fc}}{dt} = \bar{i}_g - \bar{i}_c - j\omega\, C_f\, \bar{u}_{fc}$$

$$L_{fc}\frac{d\bar{i}_c'}{dt} = \overline{u}_{fc} - j\omega L_{fc}\bar{i}_c' - \bar{i}_c R_{fc} - \overline{u}_c, \qquad (1)$$

where $\overline{u}_g$, $\overline{u}_{fc}$, $\overline{u}_c$ are space vectors of the grid, filter capacitor and converter voltages; $\bar{i}_g, \bar{i}_c$ are space vectors of the grid and converter currents; ω is the line frequency. To solve the system (1), it is necessary to express the magnetizing currents $\bar{i}_g'$and $\bar{i}_c'$ in terms of the other variables. Based on the equivalent circuit in Fig. 2, the following equations may be written:

$$\begin{aligned}\bar{i}_g' &= \frac{\bar{i}_g(R_{Feg}+R_{fg}) - \overline{u}_g + \overline{u}_{fc}}{R_{Feg}} \\ \bar{i}_c' &= \frac{\bar{i}_c(R_{Fec}+R_{fc}) + \overline{u}_c - \overline{u}_{fc}}{R_{Fec}},\end{aligned} \qquad (2)$$

where R_{Feg} and R_{Fec} are the equivalent iron losses resistances of the grid-side and converter-side inductors, respectively.

2.2 Frequency Characteristics of the LCL Filter

Stability problem of the system is related to the frequency characteristics of the LCL filter, i.e. to its resonance effect. The amplitude frequency characteristic $|I_g(j\omega)/U_c(j\omega)|$ without iron losses is calculated using the basic parameters of LCL filter listed in Tab. 1 and shown in Fig. 3 with a thin line. The resonance peak of 30 dB appears at a frequency which can be calculated as follows:

$$f_{res} = \frac{1}{2\pi}\sqrt{\frac{L_{fg}+L_{fc}}{C_f L_{fg} L_{fc}}}. \qquad (3)$$

The L filter frequency characteristic is given in Fig. 3 with dashed line. As the inductance of the L filter equals the sum of the inductances of the LCL-filter, both show the same low-frequency behavior.

To investigate the influence of the inductors iron losses the LCL filter frequency characteristic was measured using the similar procedure as in reference [9]. The grid-side inductor is short-circuited and the LCL filter is supplied through converter side terminals by a frequency converter that can deliver voltages with the fundamental frequencies of up to two kHz. The voltage amplitude is adjusted so that the current through the grid-side inductors is to be about 10 A at the measured frequencies. Based on the measured grid-side current and converter-side voltage the conductivity is calculated. The measured results are shown in Fig. 3 by crosses and it is evident that the measured frequency characteristics has significantly lower resonance peak. Assuming that the grid-side and converter-side iron losses resistances are equal, they are determined by parameters fitting to the measured frequency behavior and it gives $R_{Feg} = R_{Fec} = 95\ \Omega$. The calculated frequency characteristic with included iron losses is also shown in Fig. 3. A very good matching between calculated and measured characteristic can be seen.

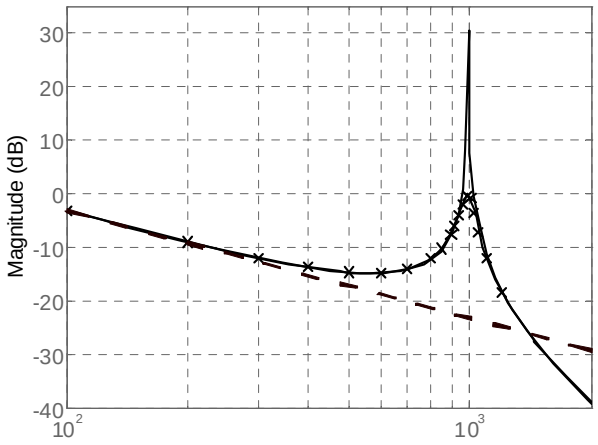

Fig. 3. Frequency characteristics of filters: - - - - - L filter; —— LCL filter without iron losses; ——LCL filter with iron losses; **xxx** *measured results*

3 CONTROL OVERVIEW AND DESIGN

The complete control structure with the converter current feedback is presented in Fig. 4. The control structure is cascaded with the outer loop which controls the DC link voltage to a constant reference u_{DC}^* using the PI controller. There are two inner current loops which are implemented in synchronous dq-rotating frame with d-axis aligned to the grid voltage space vector. The reference value of the active current component (i_d^*), which depends on a load, is generated by the DC link voltage controller. On the other hand, the reactive current reference (i_q^*) is set depending of the desired reactive power. To decouple the *d*- and *q*-current dynamics, decoupling terms $-i_d\omega L_f$ and $i_q\omega L_f$ are added to the outputs of the current PI controllers, where the measured *d*- and *q*-voltages (u_{gd},u_{gq}) are also added. The resultant signals are the *d*- and *q*-reference of the converter voltages (u_{cd}^*,u_{cq}^*). These signals are transformed to the stationary reference frame, and obtained signals ($u_{c\alpha}^*$,$u_{c\beta}^*$) are used as commands to the space vector modulation of the IGBT converter. Transformation from the synchronous rotating reference frame to the stationary reference frame ($dq \rightarrow \alpha\beta$) is performed using angle ϑ generated from the line voltages.

3.1 Current Control Loop Design

To design the PI current controller it is recommended to neglect the filter capacitor using the L approximation of the LCL filter [6]. This is possible because the dynamic behavior of the LCL filter is similar to an L filter in the low frequency range that corresponds to the current controller bandwidth. So the control plant becomes first-order delay

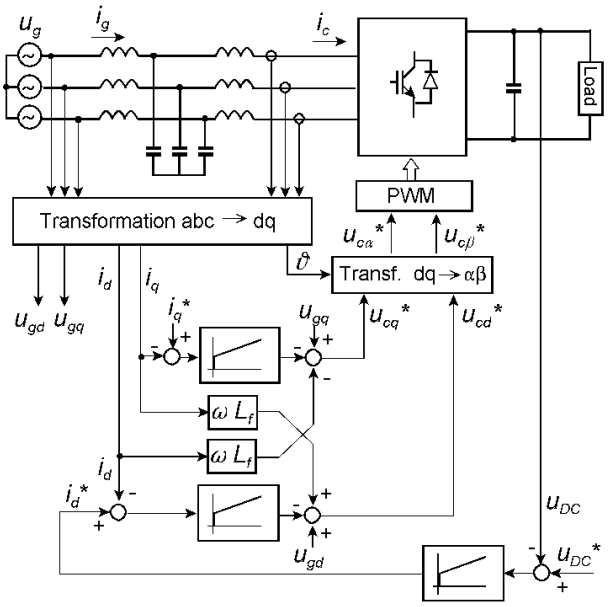

Fig. 4. Control structure of PWM converter

element with a transfer function:

$$G_f(s) = \frac{i_f(s)}{u_c(s)} = \frac{1}{R_f + L_f s}, \tag{4}$$

where $R_f = R_{fg} + R_{fc}$, $L_f = L_{fg} + L_{fc}$.

Assuming that the d- and q-current dynamics are decoupled, both current control loops are identical and can be tuned using the same parameters for the d- and q-current controllers. There are many delays in the control loop (the processing time of the algorithm, A/D conversion time, delay time of the converter) which have to be taken into account for the control design. Commonly, all delays are grouped together to form single first-order delay element with equivalent time constant (T_{eq}). The choice of T_{eq}mostly depends on the sampling time and the PWM pattern which are usually synchronized. Fig. 5 illustrates the relationship between the sampling instants and the PWM pattern implemented in the converter of the laboratory setup. The space vector modulation technique is applied to control the three-phase IGBT converter. The PWM pattern is symmetrical around the sampling instant, which makes it possible to sample ripple-free currents and, from a signal point of view, low pass filtering without delays. The computation time of the control algorithm (T_c) must be shorter than half of the sampling time (T_s) because the update of PWM is performed with the delay of the half of sampling time with respect to the sampling instant. From the control point of view it is necessary to define the total delay that varies in the range $0.5T_s$ to T_s depending on the actual control signal. Assuming the statistical delay

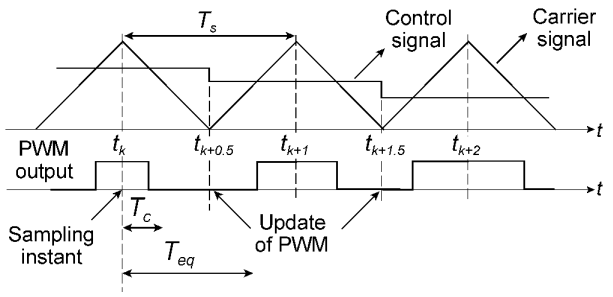

Fig. 5. Illustration of PWM pattern and equivalent time constant

of the PWM converter is $0.25T_s$ [13], the equivalent time constant $T_{eq} = 0.75T_s$.

Although the digital PI controllers are used, it is convenient to use continuous domain analysis to design it. The block diagram of the simplified current control loop is shown in Fig. 6. Assuming that the DC link voltage is kept to the constant value, variation in the grid voltage (Δu_g) is the only disturbance signal.

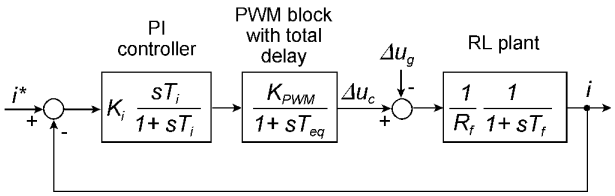

Fig. 6. Block diagram of current control loop

In the literature, the current PI controller parameters tuning is usually done using either technical [6,8] or symmetrical [5,9] optimum. The controller parameters designed according to technical optimum provides an optimal response to the step change of reference, but its drawback is slow-poor disturbance rejection. This problem is more significant in the higher ratings converter which have large filter time constants (>100 ms). Such a case is the considered system. However, due to the large time constant it is possible to use the simplified transfer function $1/sL_f$, and to choose the current PI controller parameters according to the symmetrical optimum. It gives [13]:

$$K_i = \frac{L_f}{\alpha\, K_{PWM} T_{eq}}\ , \quad T_i = \alpha^2 T_{eq}, \tag{5}$$

with typically $2 \leq \alpha \leq 3$.

3.2 DC Link Voltage Control Design

The dynamics of the DC link voltage can be expressed as [9]:

$$C_{DC}\frac{du_{DC}}{dt} = i_{DC} - i_{Load} = \frac{3u_{gd}i_{gd}}{2u_{DC}} - i_{Load}. \tag{6}$$

The choice of the DC link voltage PI controller parameters (K_{DC},T_{DC}) is based on the approximation of the inner current loop with first-order delay element using the time constant $T_{inner} = 4T_{eq}$. Considering (6), the simplified DC link voltage control loop shown in Fig. 7 is obtained. As the DC link voltage should be controlled to its constant reference, the PI controller parameters are also tuned according to the symmetrical optimum, [9]:

$$K_{DC} = \frac{2}{3}\,\frac{U_{DC}C_{DC}}{\alpha\, T_{inner}U_{gd}}\ , \quad T_{DC} = \alpha^2 T_{inner}. \tag{7}$$

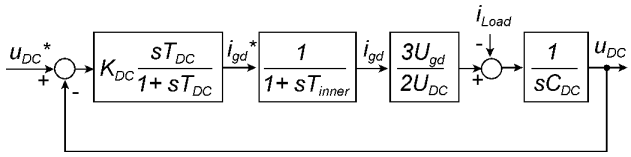

Fig. 7. Block diagram of DC link voltage control loop

4 STABILITY ANALYSIS

Although the control system of the PWM converter with LCL filter has the cascaded structure with the inner and outer loops, the inner current loop stability is of the crucial importance for the overall system stability [8,9,11]. Most papers which deal with stability problem of the PWM converter use the discrete z-domain analysis and the root locus technique. In such analyses the LCL filter model is converted to the discrete-time one and the pole placement of the closed current control loop is analyzed. All the processing delays are commonly taken into account by one sample delay what is theoretically correct if the equivalent delay time is equal to the sampling time ($T_{eq} = T_s$). However, it is mostly not true, i.e. the equivalent discrete system has the transport delay which is not an integer multiple of the sampling time. In such cases, the application of the z-domain root locus technique causes error in the stability margin determination.

In this paper, stability analyses are carried out by means of two methods. Firstly, the discrete z-domain analysis with assumed one sample delay is used for the stability limit determination. Afterwards, the nonlinear model developed in Matlab/Simulink is used.

4.1 Discrete z-domain analysis

If the converter current feedback is used, the transfer function of the LCL filter with iron losses can be derived from equations (1) and (2). It gives:

$$G_f(s) = \frac{i_c(s)}{u_c(s)} = \frac{a_3s^3 + a_2s^2 + a_1s + a_0}{b_3s^3 + b_2s^2 + b_1s + b_0}, \tag{8}$$

where the coefficients of the numerator and denominator polynomials are given in Appendix A.

The root locus analysis is based on the open loop transfer function of the current control loop. It includes system plant (8), PI current controller and delay element. To apply discrete z-domain analysis the transfer functions of the system plant and PI controller are transformed to the equivalent discrete-time transfer functions using zero order hold (ZOH) method, and delay element is taken into account by one sample delay [14].

The control system with LCL filter without included iron losses is firstly analyzed. In that case the transfer function (8) becomes simpler, and its polynomials coefficients are also given in Appendix A.

Figure 8 depicts the root locus without the inductors iron losses, where the location of the closed-loop poles depending on the proportional gain (K_i) of the current controller are shown. The calculation is performed with the integral time constant of the current controller $T_i = 2$ ms. It can be seen that the root locus has one real pole, two low frequency poles and two high frequency resonance poles. The change of poles location with increasing K_i is illustrated by arrows, and the pole locations for $K_i = 3.2$, which corresponds to symmetrical optimum, are marked. The low frequency poles are placed inside the unity circle for $K_i < 6.9$, whereas the resonance poles are outside of the unity circle for all gains. It is clear that the system would be unstable without an additional damping of the resonance poles.

To confirm the influence of iron losses on the system stability, the LCL filter with air core inductors was designed and used in the considered system. These inductors have approximately equal inductances as the iron core ones, but their resistances are much bigger ($R_{fg} = 67\ m\Omega$, $R_{fc} = 125\ m\Omega$). To construct air core inductor with the same resistance as the iron core one, the inductor size should be too large.

The resonance pole branch of the system with the LCL filter using air core inductors is shown in Fig. 9. Now, because of the increased damping, for some small gains ($K_i < 0.85$) the resonance poles are placed inside the unity circle.

The resonance pole branch obtained with taking into account the inductor iron losses ($R_{Feg} = R_{Fec} = 95\ \Omega$) is shown in Fig. 10. The real pole and low frequency pole branches are not shown because they are not significantly affected by the iron losses. The system is stable for$K_i < 2.91$, what means that the PWM rectifier with LCL filter and converter current feedback does not necessary need an additional passive or active damping, as suggested in literature [5-11]. However, because of the low proportional gain of the current controller such a system

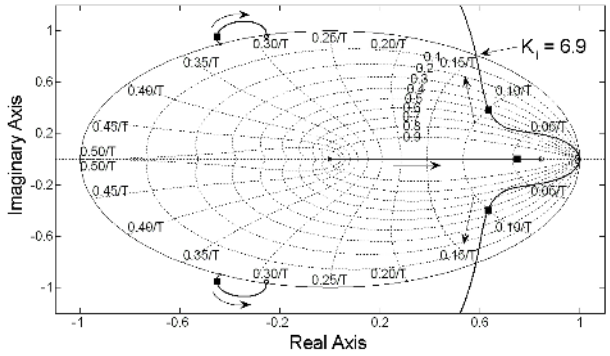

Fig. 8. Root locus of current loop without iron losses of LCL filter

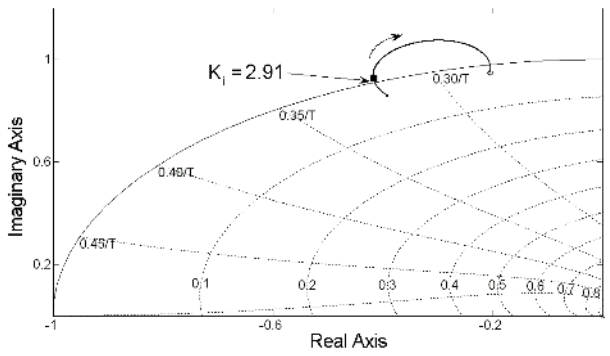

Fig. 10. Resonance pole branch with included iron losses of LCL filter

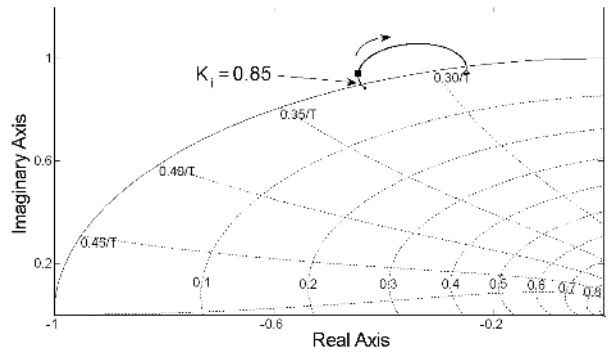

Fig. 9. Resonance pole branch of system with LCL filter using air core inductors

would not have an optimal dynamic behavior, i.e. the current response would be somewhat slower. Apart from that, as the resonance poles are close to the stability margin for these low gains, high current harmonics near the resonance frequency could appear. However, those drawbacks are not necessarily fundamental for some applications, as adjustable speed drives with the PWM converter on the grid side.

4.2 Stability Analysis by Means of Nonlinear Model

Stability analysis shown in previous subsection is based on the linear model of the LCL filter. This implies various assumptions such as: the grid voltage is the three-phase symmetrical sinusoidal voltage, all higher harmonics in the converter voltages are neglected, the equivalent delay time is equal to the sampling time, the cross-coupling effect is neglected. To investigate the influence of above simplifications and nonlinearities, which appear in the actual system, on the system stability, the nonlinear model of the system with only the inner current control loops is developed using Matlab/Simulink software package [14]. This model is shown in Fig. 11. The outer DC link voltage control loop is not modeled for the sake of comparison with the results obtained by root locus method. Thus, the DC link voltage is supposed to be constant.

The model structure is practically equal to the control block diagram shown in Fig. 4. It consists of the power and control parts. The three-phase voltage block is connected to the LCL filter through the measurement block which measures the grid voltages and currents. Besides the fundamental harmonic, the voltage block can generate higher harmonic. The LCL filter is modeled by three-phase inductances, capacitance and resistances with separate the copper and iron losses resistances. The PWM converter block consists of six IGBT-diodes switches which are in the conduction state modeled by the resistance and forward voltage. In that way the influence of IGBT/diodes conduction losses on the LCL filter resonance damping is taken into account. The PWM block generates the gate signals using the space vector modulation technique based on the reference voltages in the stationary reference frame and the DC link voltage. The delay block introduces the time delay of the half sampling time which is necessary to obtain the PWM pattern realized in the actual system (see Fig. 5). The control part of the model is realized as the discrete-time model with sampling frequency of 3 kHz. The analogue measured values of the grid voltages and converter currents are time-discretized by ZOH element. The control algorithm is previously in detail explained in Section 3.

To compare the stability margins obtained by the root locus technique, simulations are carried out for both LCL filters; with the air and iron core inductors. The LCL filter parameters are equal to the ones that are used in the root locus analysis. The fifth harmonic of the 3% is included in the supply voltage, as it was measured in the laboratory supply voltage.

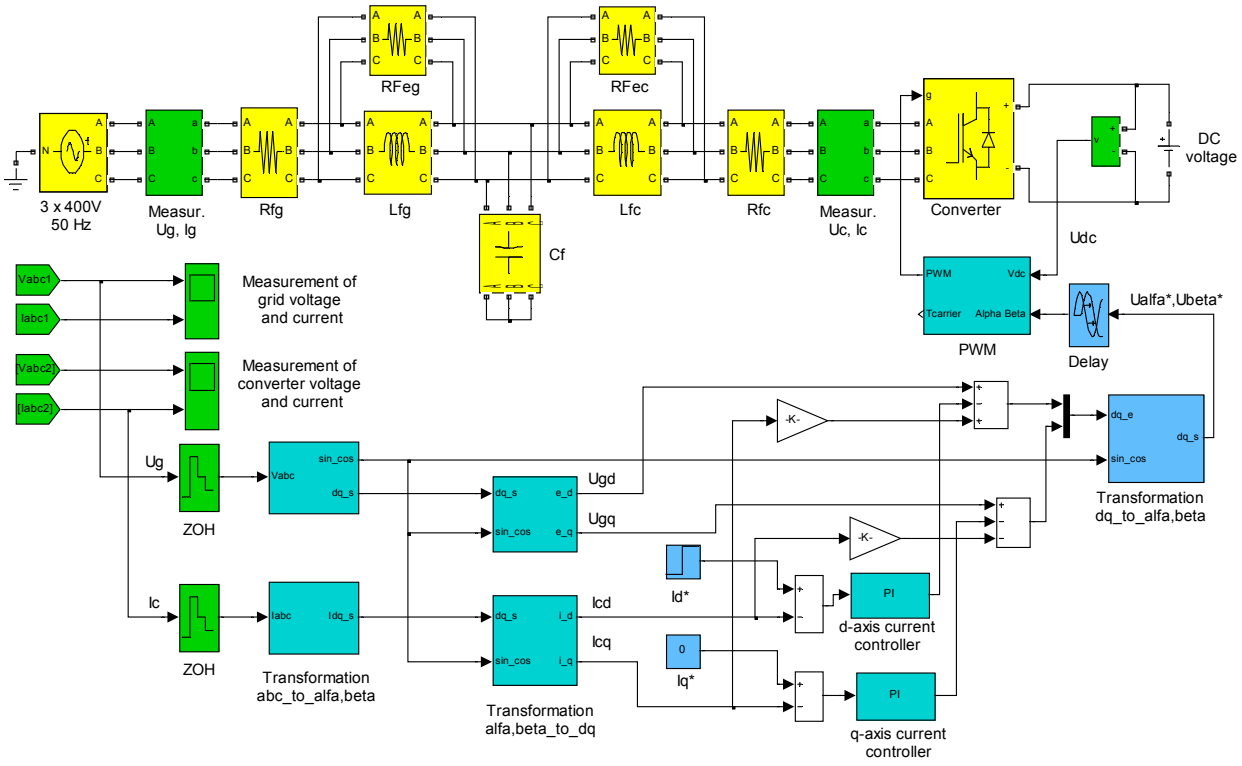

Fig. 11. Nonlinear model of system with constant DC link voltage

Figure 12 shows the grid current waveform obtained by simulation of the system with air core inductors and the current controller proportional gain $K_i = 1$. It should be noted that for $K_i = 1$ the resonance poles in root locus are placed outside the unity circle (see Fig. 9). However, although small oscillations are visible in Fig. 12, according to the nonlinear model simulation the system is stable. As shown in Fig. 13, for $K_i = 1.5$ the system approaches the stability limit. It should be noted that the critical proportional gain at which the system becomes unstable is almost two times bigger than the one obtained by the root locus analysis. This is due to the different equivalent delay times which are used in the root locus and nonlinear model analyses. Because of the modeled PWM pattern that corresponds to the one realized in the actual system (see Fig. 5), the equivalent delay time in the simulation model is less than the one used in the root locus analysis.

The simulation procedures are also carried out for the LCL filter with iron core inductors and various proportional gains of the current controllers. Fig. 14 shows the grid current for $K_i = 1.5$ that is the critical gain for the system with air core inductors. The iron losses damp the resonance oscillations and the system is stable for this gain. The current harmonic distortion is due to the fifth harmonic in the supply voltage. The stability margin is achieved for critical gain $K_i = 4.3$, as it is shown in Fig. 15. As expected, the iron losses significantly extend the range of the current controller gains for which the system is stable. Also, the critical gain obtained by the nonlinear model analysis is bigger then the one obtained with root locus analysis.

5 EXPERIMENTAL RESULTS

To validate the results of the theoretical analysis, the experimental investigations have been carried out on a 40 kW laboratory setup. It was designed and built for an induction motor adjustable speed drive in hoisting applications. The considered PWM converter with the LCL filter is the grid-side converter of this drive. For the testing of this converter in the rectifier mode of operation, the motor-side frequency converter is disconnected and a resistance load through an IGBT switch is connected to the DC link bus. The control algorithm is implemented on Texas Instruments TMS320F28335 floating point digital signal controller. All other important parameters of the PWM

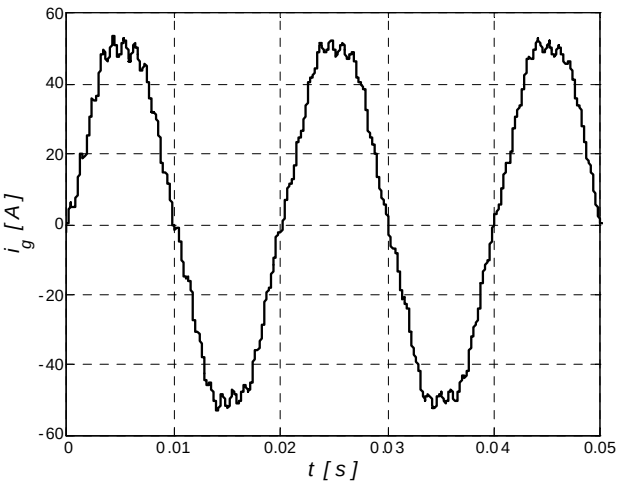

Fig. 12. Simulated grid current with LCL filter using air core inductors for $K_i = 1$

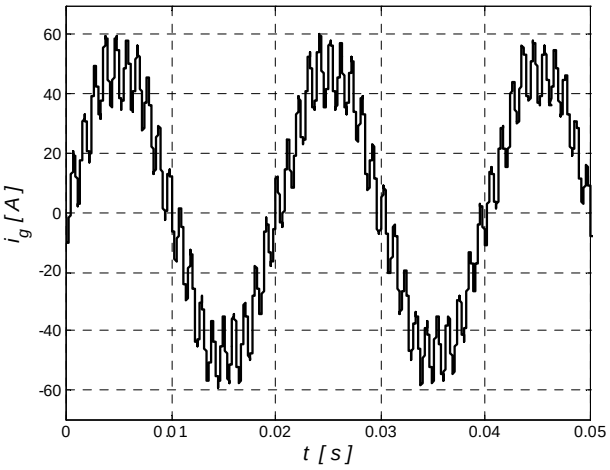

Fig. 13. Simulated grid current with LCL filter using air core inductors for $K_i = 1.5$

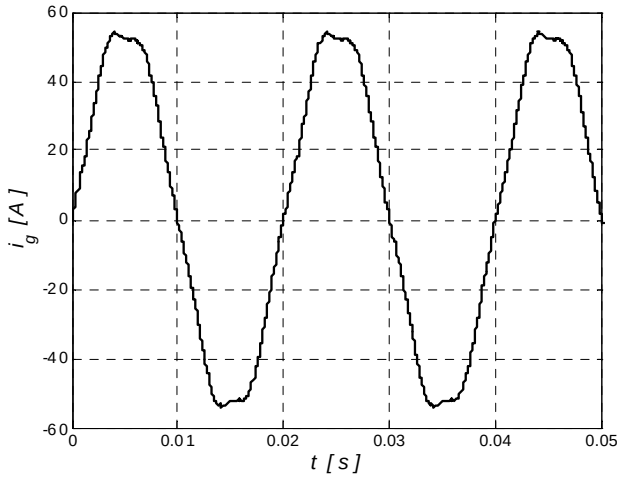

Fig. 14. Simulated grid current with LCL filter using iron core inductors for $K_i = 1.5$

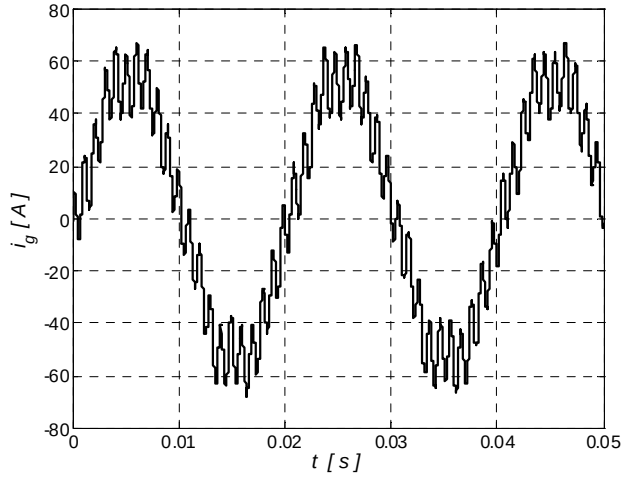

Fig. 15. Simulated grid current with LCL filter using iron core inductors for $K_i = 4.3$

converter with LCL filter are given in Table 1. The photo of the laboratory setup is shown in Fig. 16.

Figures 17 and 18 show the grid current waveforms when the LCL filter with air core inductors is used, and the PWM converter is loaded with 24 kW resistance load. The same current controller proportional gains have been set as in the corresponding simulation studies (see Fig. 12 and 13). A very good match between the simulations and measurements validates the nonlinear model.

Figures 19 and 20 show the results obtained using the LCL filter with iron core inductors for $K_i = 1.5$and $K_i = 2.1$ By comparison of the results shown in Fig. 18 and 19, it is clear that the system using LCL filter with iron core inductors becomes more stable, as it is previously concluded by theoretical analysis. Fig. 20 shows the grid current waveform and its spectra for the critical proportional gain ($K_i = 2.1$). The oscillation frequency is about 1030 Hz and it is slightly higher than the resonance frequency calculated with the nominal LCL filter parameters (985 Hz).

Although the experimental results generally confirm the theoretical analyses about the iron loss influence on the resonance pole damping, it should be noted that the stability margins obtained theoretically by nonlinear model analysis are somewhat wider. Thus, it can be concluded that the equivalent iron loss resistances of the LCL filter inductors determined by the method proposed in [9] are not reliable for the stability margins determination.

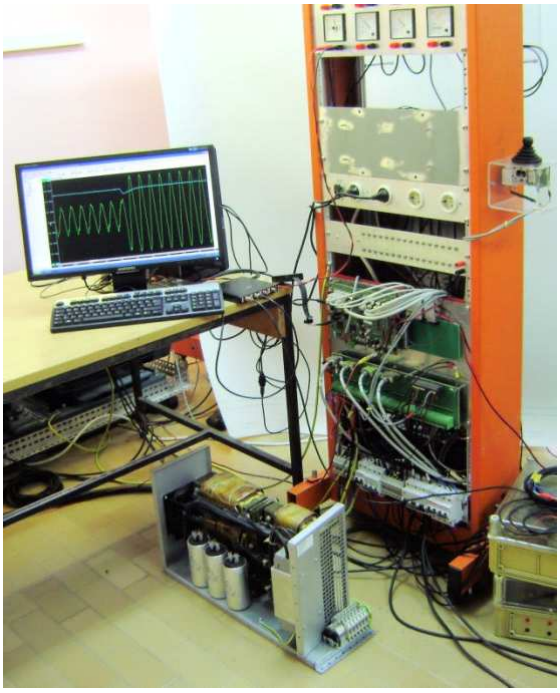

Fig. 16. Laboratory setup of PWM converter with LCL filter

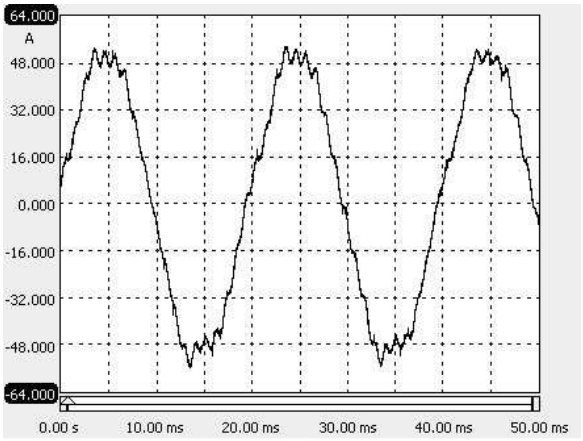

Fig. 17. Measured grid current obtained using LCL filter with air core inductors for $K_i = 1$

Figure 21 shows the responses of DC link voltage and grid current to the resistance load step change from 9 kW to 24 kW. These responses were recorded with the following parameters of the DC link voltage and current PI controllers: $K_{DC} = 1, T_{DC} = 9\,ms$, $K_i = 1, T_i = 2\,ms$. It can be seen from this figure that the response time on the load step is about 30 ms. Although, the proportional gain of the current controller has been chosen to be significantly less than the one required by the symmetrical optimum, the

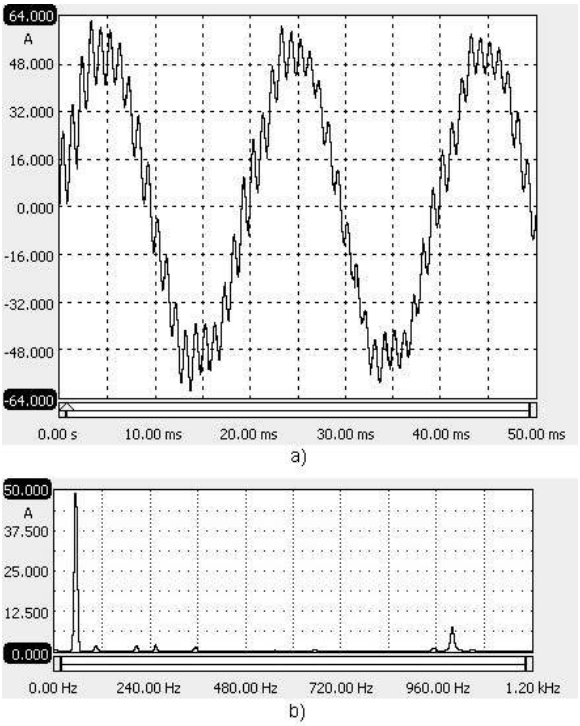

Fig. 18. Measured grid current waveform (a) and its spectra (b) obtained using LCL filter with air core inductors for $K_i = 1.5$ (stability limit)

obtained dynamic behavior is quite satisfactory for many applications. This is illustrated in Fig. 22 and 23 where the grid voltage and current of the inverter-fed induction motor drive during the dynamic motoring and regenerative mode of operations, respectively, are shown.

6 CONCLUSION

The stability problem of the three phase PWM converter with LCL filter and converter current feedback is analyzed. The comparative stability analysis is performed using two theoretical methods, z-domain root locus and nonlinear model analysis. It is shown that the stability margins obtained by means of the nonlinear model simulation are somewhat wider then the ones obtained by the root locus technique. The results obtained by the nonlinear model are confirmed by measurements.

To investigate the influence of the iron losses of the LCL inductors on the system stability, two different LCL filters are tested, with the iron and air core inductors. It is shown, theoretically and experimentally, that the system using LCL filter with iron core inductors can be stable without additional damping. For the final validation of the system stability without an additional damping the influence of different system parameters on the stability margins should be analyzed for the specific system.

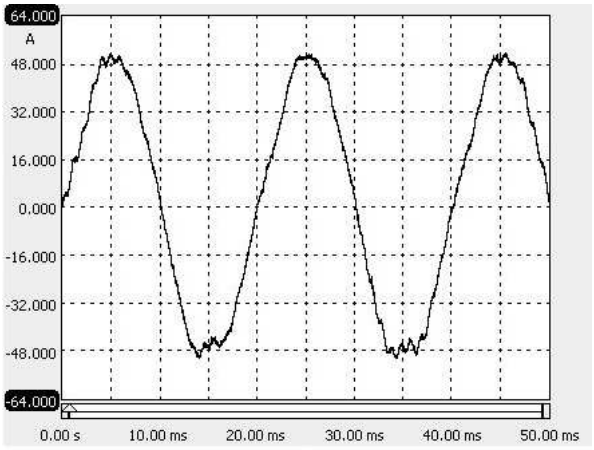

Fig. 19. Measured grid current obtained using LCL filter with iron core inductors for $K_i = 1.5$

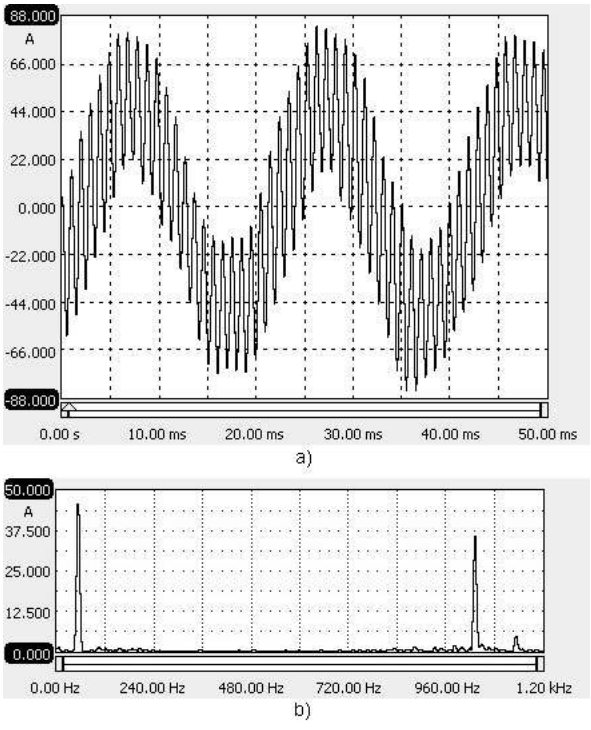

Fig. 20. Measured grid current waveform (a) and its spectra (b) obtained using LCL filter with iron core inductors for $K_i = 2.1$ (stability limit)

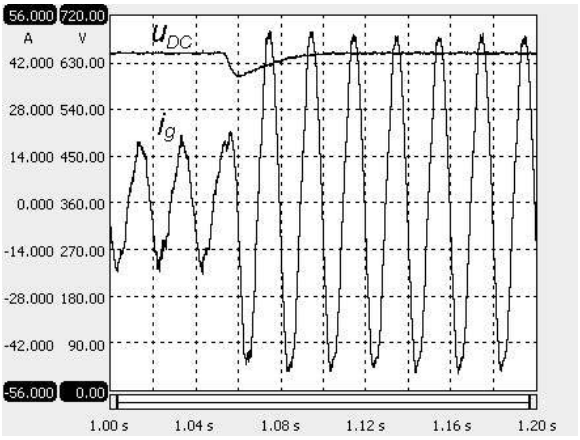

Fig. 21. Response of DC link voltage and grid current to resistance load step change from 9 kW to 24 kW

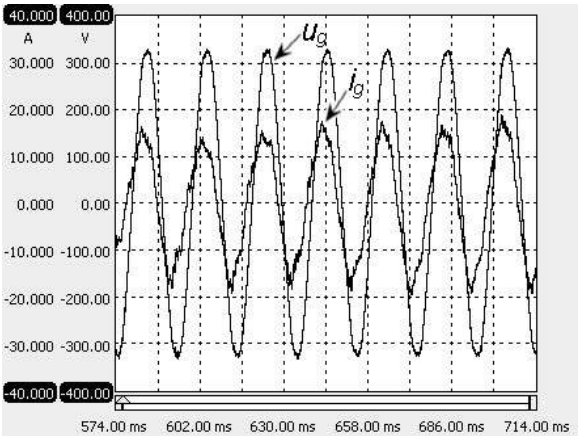

Fig. 22. Grid voltage and current of inverter-fed induction motor drive during motoring mode of operation

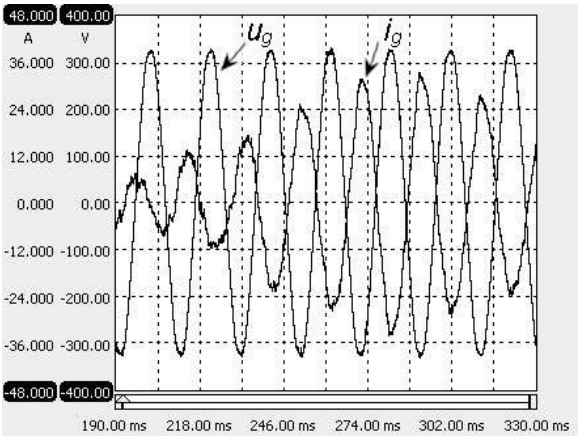

Fig. 23. Grid voltage and current of inverter-fed induction motor drive during regenerative mode of operation

APPENDIX A

If inductors iron losses of LCL filters are taken into account the polynomial coefficients of transfer function (8) are:

$$
\begin{aligned}
a_0 &= R_{Fec}R_{Feg}\\
a_1 &= R_{Fec}(L_{fg} + R_{fg}R_{Feg}C_f) + R_{Feg}L_{fc}\\
a_2 &= L_{fg}C_fR_{Fec}(R_{fg} + R_{Feg})\\
&\quad + L_{fc}(R_{fg}R_{Feg}C_f + L_{fg})\\
a_3 &= L_{fg}L_{fc}C_f(R_{fg} + R_{Feg}
\end{aligned}
$$

$$
\begin{aligned}
b_0 &= R_{Fec}R_{Feg}(R_{fc} + R_{fg})\\
b_1 &= R_{Fec}R_{fc}(L_{fg} + R_{fg}R_{Feg}C_f)\\
&\quad + L_{fc}R_{Feg}(R_{fc} + R_{Fec}) + R_{Fec}(L_{fg}(R_{fg} + R_{Feg}))\\
&\quad + L_{fc}R_{fg}R_{Feg}\\
b_2 &= L_{fg}C_fR_{Fec}R_{fc}(R_{fg} + R_{Feg})\\
&\quad + L_{fc}\left[(R_{fc} + R_{Fec})(L_{fg} + R_{fg}R_{Feg}C_f)\right.\\
&\quad \left. + L_{fg}(R_{fg} + R_{Feg})\right]\\
b_3 &= L_{fg}L_{fc}C_f(R_{fc} + R_{Fec})(R_{fg} + R_{Feg}).
\end{aligned}
$$

If the iron losses of the LCL filter are not taken into account the polynomial coefficients of transfer function (8) are:

$$
\begin{aligned}
&a_0 = 1, a_1 = R_{fg}C_f, a_2 = L_{fg}C_f, a_3 = 0,\\
&b_0 = R_{fc} + R_{fg}, b_1 = L_{fg} + L_{fc} + R_{fg}R_{fc}C_f,\\
&b_2 = C_f(R_{fg}L_{fc} + R_{fc}L_{fg}), b_3 = L_{fg}L_{fc}C_f.
\end{aligned} \tag{9}
$$

ACKNOWLEDGMENT

This work has been supported by ABB AB Crane Systems, Vasteras, Sweden.

REFERENCES

[1] M. Liserre, A. Dell'Aquila, and F. Blaabjerg, "An overview of three-phase voltage source active rectifiers interfacing the utility", *IEEE Power Tech Conference*, CityplaceBologna, 2003.

[2] F. Blaabjerg, R. Teodorescu, Z. Chen and M. Liserre, "Power Converters and Control of Renewable Energy Systems, In Proceedings of ICPE, pp. 2-20, 2004.

[3] P. Vas, "*Sensorless Vector and Direct Torque Control*", placePlaceNameOxford PlaceTypeUniversity Press, 1998.

[4] M. Liserre, F. Blaabjerg and S. Hansen, "Design and Control of an LCL-Filter-Based Three-Phase Active Rectifier", *IEEE Transactions on Industry Applications*, vol. 41, no. 5, pp. 1281-1291, 2005.

[5] V. Blasko and V. Kaura, "A Novel Control to Actively Damp Resonance in Input LC Filter of a Three-Phase Voltage Source Converter", *IEEE Transactions on Industrial Electronics*, vol. 33, no. 2, pp. 542-550, 1997.

[6] M. Liserre, A. Dell'Aquilla, and F. Blaabjerg, "Genetic Algorithm-Based Design of the Active Damping for an LCL-filter Three-Phase Active Rectifier", *IEEE Transactions on Power Electronics*, vol. 19, no.1, pp. 76-86, 2004.

[7] E. Wu and P.W. Lehn, "Digital Current Control of a Voltage Source Converter with Active Damping of LCL Resonance", *IEEE Transactions on Power Electronics*, vol. 21, no. 5, pp. 1364-1373, 2006.

[8] M. H. Bierhoff and F. W. Fuchs, "Active Damping for Three-Phase PWM Rectifiers With High-Order Line-Side Filters", *IEEE Transactions on Industrial Electronics*, vol. 56, no. 2, pp. 371-379, 2009.

[9] J. Dannehl, C. Wessels, and F. W. Fuchs, "Limitations of Voltage-Oriented PI Current Control of Grid-Connected PWM Rectifiers With LCL Filters," *IEEE Transactions on Industrial Electronics*, vol. 56, no. 2, pp. 380-388, 2009.

[10] M. Liserre, R. Teodorescu, and F. Blaabjerg, "Stability of Photovoltaic and Wind Turbine Grid-Connected Inverters for a Large Set of Grid Impedance Values, *IEEE Transactions on Power Electronics*, vol. 21, no.1, pp. 263-272, 2006.

[11] J. Dannehl, F. W. Fuchs and S. Hansen, "PWM Rectifier with LCL-filter using different Current Control Structures", in *Proceedings of Europe Conference Power Electronics Application,* Aalborg, CD-ROM, 2007

[12] R. Teodorescu, F. Blaabjerg, M. Liserre, and A. Dell'Aquila, "A stable three-phase LCL-filter based active rectifier without damping", in *Conf. Rec. IEEE IAS Annual Meeting*, pp. 1552-1557, 2003.

[13] M. Kazmierkowski, R. Krishnan, F. Blaabjerg, *"Control in Power Electronics, Selected Problems*", CityplaceOxford: Academic Press 2002, ISBN 0-12-402772-5

[14] K. Ogata, *Discrete-time control systems*, Prentice Hall International, 1995.

[15] SimPowerSystems, http://www.mathworks.com/products/ /simpower.

Božo Terzić was born in Grab, Croatia, in 1962. He received the B.Sc. and Ph.D. degrees in electrical engineering from the Faculty of Electrical Engineering, Mechanical Engineering and Naval Architecture, University of Split, Split, Croatia, in 1986 and 1998, respectively, and the M.Sc. degree from the Faculty of Electrical Engineering, University of Zagreb, Croatia, in 1993. In 1986, he became an Assistant in the Department of Electrical Power Engineering, Faculty of Electrical Engineering, Mechanical Engineering and Naval Architecture, University of Split, where, since 2009, he has been a Full Professor. Currently, he is the Head of the Department of Electric Power Engineering. His research interests include ac electrical machines and drives.

Goran Majić was born in Split, Croatia, in 1982. He received the B.Sc. degree in electrical engineering from the Faculty of Electrical Engineering, Mechanical Engineering and Naval Architecture, University of Split, Split, Croatia, in 2006. Since 2008 he has been in the Department of Electrical Power Engineering at the University of Split as a Research Assistant. He is currently working toward a Ph.D. degree in electrical engineering. His research interests include electrical machines and drives, in particular, techniques to reduce impact of grid connected PWM converters on power quality.

Alojz Slutej received his Ph.D.E.E. in 1986. M.Sc.E.E. in 1980 at the University of Zagreb, Croatia. He is employed as Global R&D Manager and works in ABB Crane Systems – Division Process Automation in Sweden. Partly, he is engaged as associate professor at the Faculty of Electrical Engineering, Mechanical Engineering and Naval Architecture, University of Split. His interest is mostly in hardware and software development in Real time controllers used for automated container cranes applications. He has been co-author of many papers published in journals and presented at national and international conferences. Alojz Slutej, Ph.D. is a member of the IFAC CCD technical committee for distributed control systems, AISE (USA Association of Iron and Steel Engineers) and KoREMA (Croatian Society for Communications, Computing, Electronics, Measurement and Control).

AUTHORS' ADDRESSES

Prof. Božo Terzić, Ph.D.
Goran Majić, B.Sc.
Department of Electric Power Engineering,
Faculty of Electrical Engineering, Mechanical Engineering and Naval Architecture,
University of Split,
Ruđera Boškovića bb, HR-21000 Split, Croatia
email: bozo.terzic@fesb.hr, goran.majic@fesb.hr

Alojz Slutej, Ph.D.
Global R&D Manager,
Crane Systems, Division Process Automation,
Tvar Leden 2,
SE-721 59 Västerås, Sweden
email: alojz.slutej@se.abb.com

Received: 2010-07-12
Accepted: 2010-10-25